NRC Research Press

ARTICLE

Collective and single-particle degrees of freedom in rotating nuclei

Anish Verma and Krzysztof Starosta

Abstract: In 1937, Hermann Jahn and Edward Teller published their research describing a mechanism of symmetry breaking in nonlinear polyatomic molecules resulting in a lifting of orbital degeneracy of an electronic state (*Proc. R. Soc. London, Ser. A* **1937**, *161*, 220), yielding insight into molecular structure. The impact of symmetry breaking on the energy and structure of quantum states is not unique to molecules and may be applied to nuclei, involving degenerate nucleon states as opposed to electronic states. Reinhard and Otten showed that the nuclear Jahn–Teller effect provides a mechanism applicable to describe the commonly observed collective quadrupole surface motion (*Nucl. Phys. A* **1984**, *420*, 173). To take into account single-particle effects, it is important to properly model the valence nucleons, especially those occupying large angular momenta orbitals near the Fermi level. In this work, a model has been developed in which two valence nucleons of the same kind are coupled to an axially symmetric quadrupole deformed rotor of the D_2 symmetry and interact through the nuclear delta force. To test this model, the band of the lowest-energy state at a given spin for ^{126}Ce is reproduced. The resultant wavefunctions are then used to calculate the g factor, reduced electric quadrupole transition probability, and spectroscopic quadrupole moment all as a function of spin. This method lays the groundwork to explore higher order symmetries following the multipole expansion.

Key words: particle-rotor model, nuclear delta force, quadrupole deformation, cerium, pair breaking.

Résumé : En 1937, Hermann Jahn et Edward Teller ont publié leur recherche décrivant un mécanisme de rupture de symétrie dans les molécules polyatomiques non linéaires qui entraîne une élévation de la dégénérescence orbitalaire d'un était électronique (*Proc. R. Soc. London, Ser. A* **1937**, *161*, 220). Ces résultats ont permis de mieux comprendre la structure moléculaire. L'effet de la rupture de symétrie sur l'énergie et les états quantiques n'est pas exclusif aux molécules et pourrait s'appliquer aux noyaux, ce qui impliquerait une dégénérescence des états des nucléons plutôt que des états électroniques. Reinhard et Otten ont montré que l'effet Jahn–Teller nucléaire s'explique par un mécanisme pouvant être appliqué à la description des mouvements collectifs quadripolaires des surfaces (*Nucl. Phys. A* **1984**, *420*, 173). Afin de tenir compte de l'effet de particule unique, il importe de modéliser correctement les nucléons de valence, en particulier ceux qui occupent des orbitales à moment angulaire de grande envergure près du niveau de Fermi. Dans le cadre des présents travaux, nous avons mis au point un modèle dans lequel deux nucléons de valence du même type sont couplés à un rotor de symétrie axiale D2 dont le quadripôle est déformé, et interagissent par la force nucléaire delta. Pour mettre à l'épreuve ce modèle, nous avons reproduit la bande de l'état de plus faible énergie du ^{126}Ce à un spin donné. Nous avons ensuite utilisé les fonctions d'onde obtenues pour calculer le facteur g, la probabilité de réduction de la transition quadripolaire électrique et le moment quadripolaire spectroscopique, tous exprimés comme une fonction du spin. Cette méthode jette les bases pour permettre l'exploration d'autres symétries d'ordre supérieur en appliquant l'expansion des multipôles. [Traduit par la Rédaction]

Mots-clés : modèle particule-rotor, force nucléaire delta, déformation quadripolaire, cérium, dissociation de paires.

Introduction

The Jahn–Teller effect plays a crucial role in chemistry, yielding insight into molecular shape through the corresponding excitation spectra, the understanding of which may be widely applied in other disciplines. Reinhard and Otten showed that the nuclear Jahn–Teller effect provides a mechanism applicable for the description of the surface motion of a deformed nucleus and subsequent impact on the regularities and patterns of excited state energies.[1] This mechanism has also been used to address nuclear phenomena including the odd–even staggering of binding energies.[2] The purpose of the presented work is to investigate the impact of the nuclear Jahn–Teller effect on the collective and single-particle degrees of freedom in atomic nuclei. This is done by use of a toy model in which certain parameters are fit to available data to obtain a wavefunctions that may be used to predict observables as a function of spin. The strong interplay of collective and single-particle degrees of freedom is unique to atomic nuclei where valence nucleon orbitals can contribute angular momenta vectors whose magnitude is on the order of six units of $\hbar$, which is comparable with the collective rotational angular momentum. Nuclear deformation follows a multipole expansion. The deformation addressed in this work corresponds to the leading-term quadrupole deformation belonging to the D_2 symmetry group.

A first-principles approach that may be applied in the description of deformed nuclei is the Hartree–Fock–Bogoliubov (HFB) cranking model. This model is well described in the literature and has seen large improvements since early work done by Inglis.[3]

Received 5 May 2017. Accepted 3 August 2017.

A. Verma and K. Starosta. Department of Chemistry, Simon Fraser University, 8888 University Drive, Burnaby, BC V5A 1S6, Canada.
Corresponding author: Krzysztof Starosta (email: starosta@sfu.ca).

This paper is part of a Special Issue entitled "50 Years of Chemistry at SFU".

This includes theoretical advances in relativistic HFB calculations as noted by Long et al.[4] However, as discussed by Hamamoto,[5] the cranking model may suffer from inaccuracies where band crossing occurs such as in the phenomena of pair breaking.

The simplest alternative model to the HFB cranking model that may address pair-breaking phenomenon is the particle-rotor model,[6] which is extended here to allow for coupling of a pair of valence nucleon of the same flavour: either a proton–proton or a neutron–neutron pair. This pair of nucleons occupying the same nuclear mean-field orbital is then coupled to a collective rotor core of the D_2 symmetry. There are different pairing interactions that may be used, some of which are explored by Yadav et al.[7] in a similar model to the one presented here. In this work, the pairing interaction between valence nucleons is achieved through the attractive nuclear delta force, which results in energetic contribution when the two valence nucleons occupy the same spatial coordinates. A comparison with the data for ^{126}Ce is presented and discussed. The wavefunctions from this model are then used to calculate g factors, electric quadrupole transition probabilities, and electric quadrupole moments all as a function of spin, where the result of the pair breaking is observed.

Theory and methods

Collective rotation of nucleons

Through the nuclear Jahn–Teller effect and spontaneous symmetry breaking, the nuclear mean field may deviate from a spherical shape and take on a deformed shape at a lower total energy. The surface of the deformed state may be described through a multipole expansion. It is seen that the lowest order deformation beyond the spherical shape corresponds to the quadrupole term, not the monopole or dipole terms, as they correspond to spherical compression and expansion or a center of mass shift, respectively. Using a linear combination of spherical harmonics, the surface of the quadrupole deformed nucleus is described by

$$(1)\qquad R(\beta,\gamma,\theta,\phi) = R_0\Big\{1 + \beta\cos(\gamma)Y_{2,0}(\theta,\phi) + \frac{1}{\sqrt{2}}\beta\sin(\gamma)[Y_{2,2}(\theta,\phi) + Y_{2,-2}(\theta,\phi)]\Big\}$$

where γ and β are deformation parameters.[8] For the case of $\gamma = 0$, eq. 1 simplifies to

$$(2)\qquad R(\beta,\gamma,\theta,\phi) = R_0[1 + \beta Y_{2,0}(\theta,\phi)]$$

which represents the axially symmetric quadrupole-deformed surface. Making use of axial symmetry, a right-handed coordinate system may be defined such that the symmetry axis of the deformed shape lies along the 3 axis, whereas two semi axes, equal in length, lie along the 1 and 2 axes. This intrinsic coordinate system is at rest with respect to the deformed shape. To describe rotations, a second right-handed coordinate system called the lab frame may be defined, whose axes are denoted as x, y, and z, in which the deformed shape is free to rotate (Fig. 1). Using these two coordinate systems, rotations are characterized employing a set of Euler angles $(\varphi_E, \theta_E, \psi_E)$, where the convention here is shared with Bohr and Mottelson.[9]

For the axially symmetric rotor, the semi-classical Hamiltonian takes the form

$$(3)\qquad H = \frac{\hat{R}_1^2}{2\mathcal{I}_{11}} + \frac{\hat{R}_2^2}{2\mathcal{I}_{22}} + \frac{\hat{R}_3^2}{2\mathcal{I}_{33}}$$

where $\hat{R}_k$ is the kth component of angular momentum R of the rotor, and $\mathcal{I}_{kk}$ is the corresponding moment of inertia in the intrinsic principal-axes frame. The moments of inertia here will be taken to be irrotational flow moments of inertia, as opposed to rigid body moments of inertia. This choice is to correspond to microscopic theories of the nucleus and to be consistent with previous work.[8] From this, the moments of inertia take the form

Fig. 1. The two coordinate frames are pictured, where the intrinsic frame has its axes denoted by 1, 2, and 3, whereas the lab frame has its axes denoted by x, y, and z. Note that the intrinsic frame is fixed to a body and is free to rotate about the origin shared between the two coordinate systems. [Colour online.]

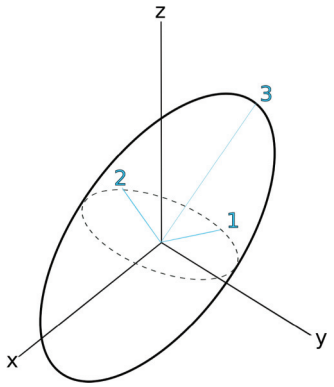

$$(4)\qquad \mathcal{I}_{kk} = \mathcal{I}_0\sin^2\left(\gamma - k\frac{2\pi}{3}\right) \qquad k = 1,2,3 \qquad \mathcal{I}_0 = 4B\beta^2$$

where B is a mass parameter, and k once again corresponds to the intrinsic coordinate system's axes. For the case of the axial rotor and $\gamma = 0$, it is seen that $\mathcal{I}_{33}$ is 0, which implies that $\hat{R}_3 = 0$, as otherwise the solution of eq. 3 leads to infinity. This cannot be the case as the energies resultant from the Hamiltonian must be finite to be physical. Similarly, along the semi-axes, the moments of inertia are $\mathcal{I}_{11} = \mathcal{I}_{22} = (3/4)\mathcal{I}_0$. Incorporating this, the Hamiltonian becomes

$$(5)\qquad H = \frac{2}{3}\left[\frac{\hat{R}^2}{\mathcal{I}_o}\right]$$

where now the numerator becomes the total angular momentum squared for the deformed nucleus. Thus, a wavefunction that describes the rotor may be chosen to be an eigenfunction of the squared angular momentum operator, so the Hamiltonian is diagonal in this basis. This naturally leads to the Wigner $D^R_{MK}(\phi_E, \theta_E, \psi_E)$ function — a function of the Euler angles, relating the lab frame to the intrinsic frame. The quantum numbers R, M, and K correspond to the total rotor angular momentum, its projection onto the z axis in the lab frame, and its projection onto the 3 axis in the intrinsic frame, respectively.

It is important to note, however, that the Wigner functions alone do not in general reflect the symmetry of the shape defined by eq. 2. Note that for an axially symmetric rotor with irrotational flow moment of inertia, the total angular momentum is perpendicular to the symmetry axis. As a result, the essential symmetries are the $\hat{R}(\boldsymbol{e}_1, \pi)$ invariance under a π rotation about the 1 axis, selected as the axis of rotation, and invariance under the identity operation $\mathbb{I}$. These two symmetry operations form a group, which is a subgroup of the D_2 symmetry group for a general quadrupole-deformed rotor. The states belonging to the fully symmetric representation of this subgroup are constructed using

$$(6)\qquad \hat{S} = \mathbb{I} + \hat{R}(\boldsymbol{e}_1, \pi)$$

Fig. 2. A comparison of energies of the lowest-energy state at a given spin measured in ^{126}Ce (red crosses) and calculated using axial rotor predictions of eq. 5 (blue circles). The parameter of $B\beta^2$ = 5.9 $\hbar^2$/MeV was extracted from the energy of the first excited state as given by eq. 10. [Colour online.]

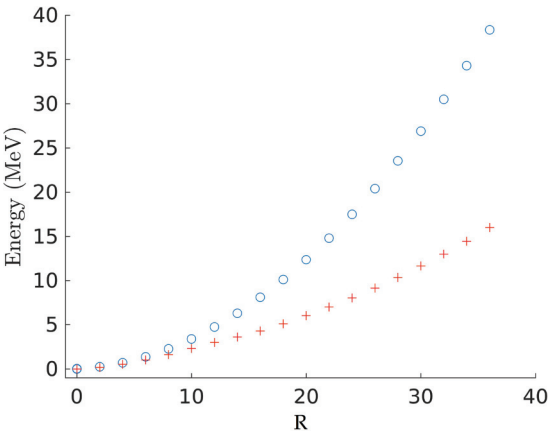

The operator $\hat{S}$ applied to the Wigner D^R_{MK} functions yields the wavefunctions for the physical states of the rotor, which, when normalized, are

$$|RMK\rangle = \frac{1}{\sqrt{1+\delta_{K,0}}}\sqrt{\frac{2R+1}{16\pi^2}}\left[D^R_{MK} + (-1)^R D^R_{M\bar{K}}\right] \quad (7)$$

However, as discussed above, $I_{33} = 0$ implies $K = 0$, thus the wavefunction of eq. 7 simplifies to

$$|RM0\rangle = \frac{1+(-1)^R}{2}\sqrt{\frac{2R+1}{8\pi^2}}D^R_{M0} = \frac{1}{\sqrt{2\pi}}Y_{RM}(\phi_E, \theta_E) \quad (8)$$

R even

The eigenvalues E_R of the Hamiltonian of eq. 5 are

$$E_R = R(R+1)\frac{2\hbar^2}{3\mathcal{I}_0} = \frac{\hbar^2}{6B\beta^2}R(R+1) \quad (9)$$

which yields for the first excited state of $R = 2$ the energy of

$$E_2 = \frac{\hbar^2}{B\beta^2} \quad (10)$$

This rotor model describes well the low-lying excited states in nuclei of certain deformed mass regions, far from the closed nuclear shells in which the spherical shell model tends to fail. However, in comparing with the data available,[10] it is evident that this model begins to fail for excited states of high angular momenta. A specific example is presented in Fig. 2, which compares energies of the lowest-energy state at a given spin measured in ^{126}Ce with the axial rotor predictions of eq. 5. The parameter $B\beta^2$ for the comparison in Fig. 2 is extracted from the energy of the first excited state according to eq. 10. Although the experimental and calculated trend in excitation energy as a function of spin is in reasonable agreement up to spin R ~ 8, the deviation at higher spins is evident. This deviation indicates missing degrees of freedom in the collective rotor model discussed so far.

Single-particle degrees of freedom

The purpose of this section is to introduce tools for handling single-particle degrees of freedom that may provide a way to address the shortcomings of the collective rotor model discussed above.

Spherical mean field

As a starting point, we assume existence of shell structure in a spherical nuclear mean field with strong spin-orbit coupling. In this potential, the subshells are formed by coupling the orbital angular momentum substates of nucleon i, $|l_i m_{li}\rangle$, to its spin substates, $|s_i m_{si}\rangle$, yielding the total angular momentum substates $|j_i\Omega_i\rangle$, explicitly as

$$|j_i\Omega_i\rangle = \sum_{m_{li},m_{si}} \langle l_i m_{li} s_i m_{si}|j_i\Omega_i\rangle\,|l_i m_{li}\rangle\,|s_i m_{si}\rangle \quad (11)$$

where $\langle l_i m_{li} s_i m_{si}|j_i\Omega_i\rangle$ is the Clebsch–Gordan coefficient, taking nonzero values for when $\Omega_i = m_{li} + m_{si}$. All of these quantum numbers follow the convention as in previous work,[9] indexed according to the nucleon to which it corresponds.

Pair of valence nucleons

Next, we consider a pair of valence nucleons outside a closed shell. In this scenario, all nucleons other than the valence nucleons occupy full shells and play no role other than to form a spherical mean field in which the two valence nucleons inhabit and may interact only with each other. In other words, the core is non-interacting, and only the pair of valence nucleons above the Fermi level may interact.

The wavefunction of a pair of nucleons must then be constructed by noting it is the coupled wavefunction of two nucleons, each with their own quantum numbers. The wavefunction for this pair must satisfy the Pauli exclusion principle and thus must be antisymmetric under the exchange of indices. To accomplish this, first consider the coupled wavefunction

$$|J\Omega\rangle = \sum_{\Omega_1,\Omega_2} \langle j_1\Omega_1 j_2\Omega_2|J\Omega\rangle\,|j_1\Omega_1\rangle\,|j_2\Omega_2\rangle \quad (12)$$

An antisymmetrized wavefunction may be constructed using the symmetry properties of the Clebsch–Gordan coefficients[11] as

$$|\Psi J\Omega\rangle = \frac{1-(-1)^{j_1+j_2-J}}{2}|J\Omega\rangle \quad (13)$$

It is important to note here that due to the antisymmetrization of the wavefunction, only even values of total angular momentum J are permitted for $j_1 = j_2 = j_0$, namely two nucleons of the same kind occupying the same subshell. Indeed, for $j_1 = j_2 = j_0$, the first term of eq. 13 takes values of 0 for odd values of J and 1 for even values of J. Explicitly, this is resultant from the fact that the quantum numbers j_1 and j_2 are half odd integers, whereas J is a whole integer value.

Nuclear delta force

The nuclear delta force models the interactions of two nucleons as a contact force, for when the nucleons occupy the same spatial coordinates in analogy to two colliding points that otherwise have no interaction (Fig. 3). This is realized through the following functional form of the Hamiltonian

$$H_\delta = V_\delta\delta(\boldsymbol{r}_1 - \boldsymbol{r}_2) \quad (14)$$

Fig. 3. A schematic diagram of the nuclear delta force and its energetic contribution for when two nucleons occupy the same spatial coordinates. Here, the spherical nucleus was chosen, as the core is non-interacting, and is a good example in which to build a framework and study this contact force to be used later in the two-particle rotor model. [Colour online.]

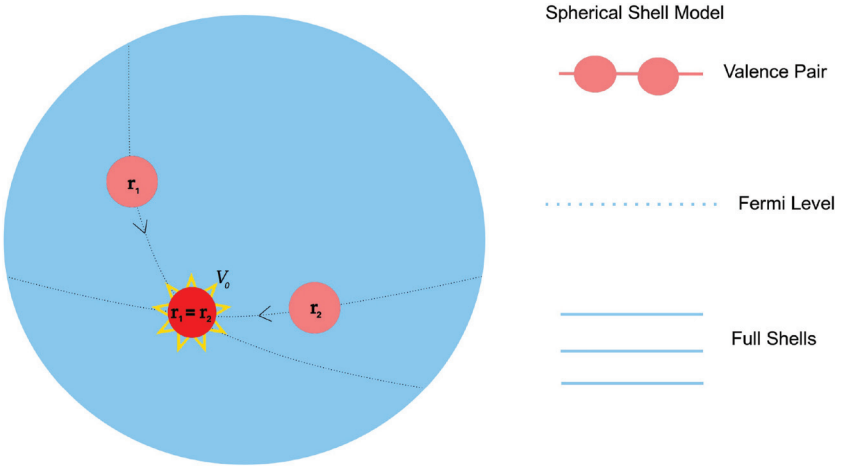

where $\delta(\boldsymbol{r}_1 - \boldsymbol{r}_2)$ is the Dirac delta function over all spatial coordinates. Here, $\boldsymbol{r}_i$ corresponds to the position of nucleon i, and V_δ is the magnitude of the interaction potential. The sum of the spherical mean field and the interaction energy is thus purported to be able to model the excited states in nuclei with a valence pair outside a closed proton and neutron shells through the Hamiltonian

$$H = H_{\text{SMF}} + H_\delta \tag{15}$$

where H_{SMF} is the spherical mean field Hamiltonian. Applying separation of variables for the Dirac delta in spherical coordinates, the matrix elements of the Hamiltonian of eq. 15

$$\langle \Psi J'\Omega' | H | \Psi J\Omega\rangle = \langle \Psi J'\Omega' | H_{SMF} | \Psi J\Omega\rangle + \langle \Psi J'\Omega' | H_\delta | \Psi J\Omega\rangle \tag{16}$$

may be found, as

$$\langle \Psi J'\Omega' | H | \Psi J\Omega\rangle = (E_1 + E_2)\delta_{J'J}\delta_{\Omega'\Omega}\delta_{j_1'j_1}\delta_{j_2'j_2} + \frac{1-(-1)^{j_1+j_2-J}}{2}\frac{1-(-1)^{j_1'+j_2'-J'}}{2} \times \chi_\delta \langle J'\Omega' | \delta(\theta_1 - \theta_2)\delta(\phi_1 - \phi_2) | J\Omega\rangle \tag{17}$$

where χ_δ is the radial term determined by the coupled radial wavefunction $|\mathcal{R}\rangle$, and scaled by V_δ

$$\chi_\delta = V_\delta \langle \mathcal{R}' | \delta(r_1 - r_2) | \mathcal{R}\rangle \tag{18}$$

The first term in the right-hand side of eq. 17 is simply the sum of single-particle energies of the nucleon pair in the spherical mean field. Below, we consider two nucleons occupying the same subshell, thus $j_1' = j_1 = j_2' = j_2 = j_0$, which implies $E_1 + E_2 = 2E_0$. The goal is to predict energies of excited states relative to the ground state; because $2E_0$ is a constant that does not influence these predictions, it can be set to zero.

Next, the angular delta functions may be expanded in terms of spherical harmonics[12] as

$$\delta(\theta_1 - \theta_2)\delta(\phi_1 - \phi_2) = \sum_{\lambda=0}^{\infty}\sum_{\mu=-\lambda}^{\mu=\lambda} Y_{\lambda\mu}(\theta_1, \phi_1)Y^*_{\lambda\mu}(\theta_2, \phi_2) \tag{19}$$

The separation of the angular delta function into the sum of products of two spherical harmonics, with each harmonic dependent on variables specific to a single nucleon of the pair, allows the matrix element of the second term in the right hand side of eq. 17 to be evaluated using multipole moments of $|j\Omega\rangle$ single-particle orbitals in the spherical mean field. The angular momentum algebra, arising from applying eq. 19 to eq. 17 results in the matrix element being fully diagonal in the pair basis of eq. 13.

The prediction from the above model is compared in Fig. 4 with experimental data[13] on low-energy excited states in ^{134}Te, which is a nucleus with two protons outside the closed proton shell at $Z = 50$ and closed neutron shell at $N = 82$. The constant parameter χ_δ for this comparison was fitted using the least squares method. It is seen that only even values of total angular momentum J are predicted with a decreasing energy gap between successive excited states, which is in general agreement with the data. One should note that there are no Coulombic effects involved in this simple model. This approximation comes from the fact that the Coulomb interaction within a nucleus is significantly weaker than the strong force interaction modelled by the spherical mean field and the contact force and thus negligible for the purposes of current work.

Deformed mean field

Next, let us consider the consequences of deformation of the mean field starting with examining the impact on a single valence nucleon and progressing to the analysis of the impact on a pair of nucleons. To model single-particle motion in a deformed mean field, a term proportional to the deformed density may be added on to the spherical mean field Hamiltonian

$$H = H_{\text{SMF}} + H_\beta \tag{20}$$

Here, the Hamiltonian H_β is defined by the density profile, assuming the validity of density functional theory. The Hamiltonian H_β for quadrupole deformation of eq. 1 takes the form

$$H_\beta = \beta\chi_\beta\left\{\cos(\gamma)Y_{2,0}(\theta,\phi) + \frac{1}{\sqrt{2}}\sin(\gamma)[Y_{2,2}(\theta,\phi) + Y_{2,-2}(\theta,\phi)]\right\} \tag{21}$$

with χ_β denoting the product of the radial matrix element and a new coupling constant scaling the interactions between the valence nucleon and the deformed core. Further, if $\chi_\beta > 0$, the valence nucleon is of particle character, whereas if $\chi_\beta < 0$, it is of hole character. For the axially symmetric shape of $\gamma = 0$, eq. 21 simplifies to

Fig. 4. Excitation energy with respect to the ground state for two valence protons in the $1g_{7/2}$ shell in ^{134}Te as measured (red crosses) and predicted (blue circles) by the spherical mean field plus a contact force model. The coupling constant of eq. 18 was fit to the experimental data using the least squares method yielding $\chi_\delta = -5.6$ MeV. [Colour online.]

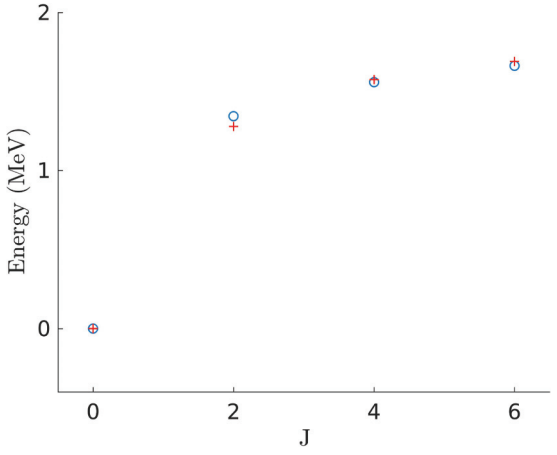

$$H_\beta = \beta\chi_\beta Y_{2,0}(\theta, \phi) \quad (22)$$

For two identical valence nucleons, eq. 22 must be of both spatial coordinates, yielding

$$H_\beta = \beta\chi_\beta[Y_{2,0}(\theta_1, \phi_1) + Y_{2,0}(\theta_2, \phi_2)] \quad (23)$$

In this work, the rotor is taken to be axially symmetric and prolate-deformed with $\beta > 0$. As a result, the positive or negative sign of $\beta\chi_\beta$ is determined by whether the nucleon is of particle or hole character, respectively. The energies resultant from diagonalizing H_β in the basis of eq. 13 for two nucleons in the $h_{11/2}$ shell are plotted as a function of $\beta\chi_\beta$ in Fig. 5. Note that H_β is diagonal in Ω but is not diagonal in J, which results in the energies having contributions from different basis states. The presence of the deformed mean field splits the energies, where the gap between these split levels is determined by the magnitude of $\beta\chi_\beta$.

Deformed mean field with the nuclear delta force

It is of interest to explore the effect of the nuclear delta force with the deformed mean field on a pair of identical valence nucleons. This is achieved by the diagonalization of the Hamiltonian $H_\beta + H_\delta$ in the basis of eq. 13 as a function of $\beta\chi_\beta$, with $\chi_\delta = -8.0$ MeV, as plotted in Fig. 6. In this figure, the energies have contributions from basis states with different values of J and Ω, because $H_\beta + H_\delta$ is nondiagonal in the basis of eq. 13. By examining the wavefunctions obtained from the diagonalization, the energies are labeled in Fig. 6 according to the basis states with the dominant amplitudes. It is seen that H_δ has the action of separating the energetic contributions by angular momentum J as was seen in Fig. 4 for ^{134}Te and that the splitting of levels from H_β is present. It is evident that the nuclear delta force plays the dominant role when compared with the deformed mean field, given that the gap between each of J is significantly greater than the splitting due to the deformed mean field. Moreover, the $J = 0$ state is significantly lower in energy than the other states. The latter result becomes very important in the particle-rotor model, which couples a nucleon pair to a deformed rotor, as it changes the energy required to keep the pair coupled to spin $J = 0$. Because the $J = 0$ state is lowest in energy, it is important to consider, as the lowest-energy band is addressed by the calculations developed in this paper. The above results imply that energy is needed to decouple the pair from $J = 0$.

Fig. 5. The energies resultant from the diagonalization of H_β in the basis of eq. 13 for two nucleons in the $h_{11/2}$ shell as a function of the coupling constant $\beta\chi_\beta$. For $\beta > 0$, positive $\beta\chi_\beta$ corresponds to particle character for the valence pair and negative $\beta\chi_\beta$ corresponds to hole character for the valence pair. [Colour online.]

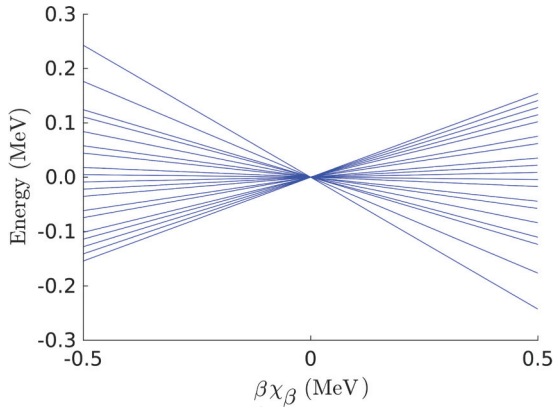

Fig. 6. The energies resultant from the diagonalization of $H_\beta + H_\delta$ in the basis of eq. 13 for two nucleons in the $h_{11/2}$ shell as a function of the coupling constant $\beta\chi_\beta$, with $\chi_\delta = -8.0$ MeV. The energies are labeled based on the dominant amplitudes in the wavefunctions resultant from the diagonalization. [Colour online.]

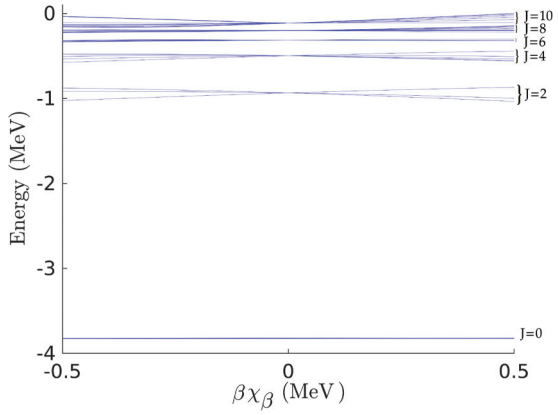

Pair-rotor coupling model

In this section, a model is developed for two identical nucleons coupled to an axially symmetric quadrupole deformed rotor with the intention to remedy the deviations observed in Fig. 2 between the experimental data and the pure axial rotor model. This deviation was understood previously as a consequence of single-particle degrees of freedom missing in the pure axial rotor model. Both, single-particle and collective degrees of freedom are included in the model discussed in the current section.

The total angular momentum $\boldsymbol{I}$ for the rotor plus a pair is

$$\boldsymbol{I} = \boldsymbol{R} + \boldsymbol{J} \qquad \boldsymbol{J} = \boldsymbol{j}_1 + \boldsymbol{j}_2 \quad (24)$$

The transformation between the lab and the intrinsic coordinate systems is again given by the Wigner D function, but now an important distinction is made. Instead of the rotor's angular momentum quantum number R defining the order of the Wigner D function, the total angular momentum quantum number, I, must take its place. This is due to $\boldsymbol{R}$ not being conserved when the rotor

is coupled to two particles with angular momenta $\boldsymbol{j}_1$ and $\boldsymbol{j}_2$ respectively. However, the total angular momentum $\boldsymbol{I}$ is conserved and defines the transformation between coordinate systems of interest.

The model wavefunctions include the direct products of the aforementioned Wigner D functions and pair wavefunctions of eq. 13. These products need to be properly symmetrized to account for symmetries of the rotating deformed mean field. For the collective rotor alone, the symmetry operator of eq. 6 was fully defined by the identity and the $\hat{R}(e_1,\pi)$ rotation. Given that the current model adds two extra particles, the symmetry operators must be modified based on the substitution $\boldsymbol{R} = \boldsymbol{I} - \boldsymbol{J}$, resultant from eq. 24. The rotation operator will rotate the pair and the rotor by π, while simultaneously rotating the pair by $-\pi$, yielding

$$\hat{R}^R(e_1,\pi) = \hat{R}^I(e_1,\pi)\hat{R}^J(e_1,-\pi) \tag{25}$$

where the superscript indicates on which part of the system the rotation is acting. Applying the symmetry operator to the product wavefunction and normalizing the result yields for the model wavefunction

$$|IMKj_1j_2J\Omega\rangle = \frac{1-(-1)^{j_1+j_2-J}}{2}\sqrt{\frac{2I+1}{16\pi^2(1+\delta_{\Omega,0})}} \times \left[D^I_{MK}|J\Omega\rangle + (-1)^{I-J}D^I_{M\bar{K}}|J\bar{\Omega}\rangle\right] \tag{26}$$

with $\Omega \in [-J, J]$ and $K \in [-I, I]$. Equation 26 is effectively the wavefunction of a rotor coupled to a single "super" particle with quantum numbers J and Ω, with the restriction on even J for $j_1 = j_2$ that arises from antisymmetrization.

Subsequently, the rotor Hamiltonian must be modified to incorporate the two valence nucleons, by explicitly using the substitution of eq. 24, which yields

$$H_{\text{Rot}} = \frac{[\hat{I}_1 - \hat{J}_1]^2}{2\mathcal{I}_{11}} + \frac{[\hat{I}_2 - \hat{J}_2]^2}{2\mathcal{I}_{22}} + \frac{[\hat{I}_3 - \hat{J}_3]^2}{2\mathcal{I}_{33}} \tag{27}$$

The special case of the irrotational flow moment of inertia for axial symmetry at $\gamma = 0$ with $\mathcal{I}_{11} = \mathcal{I}_{22} = (3/4)\mathcal{I}_0$ and $I_{33} = 0$ implies for physical solutions $\hat{I}_3 = \hat{J}_3$, which reduces eq. 27 to

$$H_{\text{Rot}} = \frac{2}{3\mathcal{I}_0}\left[[\hat{I}_1 - \hat{J}_1]^2 + [\hat{I}_2 - \hat{J}_2]^2\right] \tag{28}$$

Furthermore, the $\hat{I}_3 = \hat{J}_3$ condition implies for wavefunctions of eq. 26 that $\Omega = K$, yielding for $j_1 = j_2 = j_0$, the model wavefunction of

$$|IMj_0j_0J\Omega\rangle = \sqrt{\frac{2I+1}{16\pi^2(1+\delta_{\Omega,0})}} \times \left[D^I_{M\Omega}|J\Omega\rangle + (-1)^{I-J}D^I_{M\bar{\Omega}}|J\bar{\Omega}\rangle\right] \quad J \text{ even} \tag{29}$$

Expanding and simplifying, the model Hamiltonian becomes

$$H_{\text{Rot}} = \frac{2\hbar^2}{3\mathcal{I}_0}\left[\hat{I}^2 - \hat{I}_3^2 + \hat{J}^2 - \hat{J}_3^2\right] + \frac{4\hbar^2}{3I_0}[\hat{I}_{+1}\hat{J}_{-1} + \hat{I}_{-1}\hat{J}_{+1}] \tag{30}$$

Here, the first term in the right-hand side of eq. 30 is completely diagonal in the basis of wavefunctions of eq. 29, whereas the second term is not. This second term is the Coriolis coupling term[14] to which an ad hoc attenuation term is sometimes applied in the literature to better agree with the data for a wider range of

Fig. 7. A comparison of energies of the lowest-energy state at a given spin measured in ^{126}Ce (red crosses) and calculated using the Hamiltonian of eq. 32 (blue circles). The valence nucleon pair is assumed to occupy the $h_{11/2}$ proton subshell. The fitted model parameters are $\beta\chi_\beta = 0.2$ MeV, $\chi_\delta = -8.0$ MeV, and $B\beta^2 = 8.9\ \hbar^2$/MeV. [Colour online.]

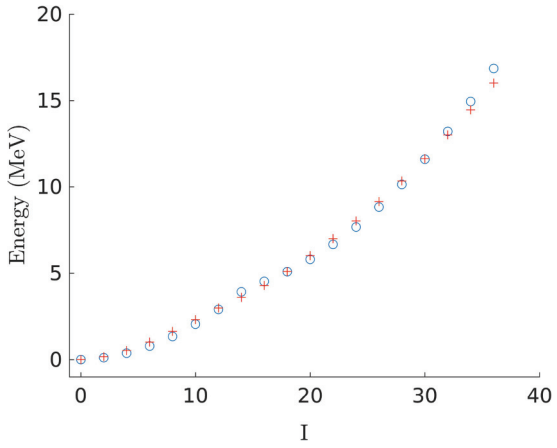

total angular momentum. Thus, the Hamiltonian may be written as

$$H_{\text{Rot}} = H_{\text{Diagonal}} + H_{\text{Coriolis}} \tag{31}$$

Pair-rotor coupling model for interacting nucleons

The Hamiltonian incorporating the interaction of the valence pair with the deformed mean field and the contact interactions between valence nucleons takes the form

$$H = H_{\text{Diagonal}} + H_{\text{Coriolis}} + H_\beta + H_\delta \tag{32}$$

with H_β being the deformed mean field Hamiltonian and H_δ being the delta force Hamiltonian, with all terms of eq. 32 discussed in the previous sections of this paper. The Hamiltonian of eq. 32 is diagonalized numerically in the basis of wavefunctions of eq. 29. A set of lowest-energy states at a given spin for the axially deformed nucleus of ^{126}Ce is chosen and compared with the model calculations. The results are shown in Fig. 7. The three model parameters are as follows: the parameter for the moment of inertia $B\beta^2$, the deformed mean field coupling constant $\beta\chi_\beta$, and the delta force Hamiltonian coupling constant χ_δ. These three parameters were adjusted via the least squares minimization technique to fit the experimental data. The fit parameters are given in caption of Fig. 7, and specifically for the delta force Hamiltonian, $\chi_\delta = -8.0$ MeV, agreeing with the range parameters found for the delta force in the spherical nucleus. The mass parameter for the moment of inertia is larger than what is expected from a pure rotor model of eq. 10. Now, note that for Fig. 7, predicted trends are with good agreement with the data but deviate from the parabolic trend expected for a pure collective rotor. Specifically, a distinct second parabolic trend is observed at higher values of total angular momentum at and above $I = 16$. This is the result of the Coriolis force acting on the valence particles, as the total angular momentum of the system increases. This Coriolis force favours the alignment of the angular momentum of the nucleons along the rotor angular momentum, i.e., the axis perpendicular to the symmetry axis of the mean field. This eventually leads to pair breaking, decoupling the pair from $J = 0$. However, this effect is weak at low values of the total angular momentum and cannot align the angular momentum of the pair for low spin states. It is for this reason that pair breaking appears only at higher values of angular momentum. Recall that the Coriolis force acts to align the angular

Fig. 8. From the theoretical model predictions, the two parabolic bands, pink and purple circles, respectively, are plotted. Note that there is a band crossing between $I = 14$ and $I = 16$, the location of the pair breaking between the valence protons. [Colour online.]

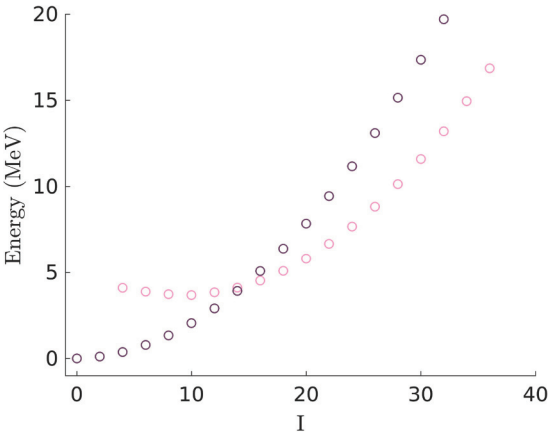

momentum of the pair with the axis of rotation, effectively decoupling the pair from $J = 0$. However, the dominant force that acts to keep the pair coupled to spin $J = 0$ is the nuclear delta force, given that the coupling constant χ_δ is significantly larger than the deformed mean field coupling constant $\beta\chi_\beta$. Effectively, this contact force acts as a pair coupling force that lowers the energy of the system for the $J = 0$ coupling such that energy is required to decouple the pair from spin $J = 0$. By means of incorporating these single-particle effects into the model, a good agreement with the data are achieved.

Using the model predictions, the two parabolic trends that meet between $I = 14$ and $I = 16$ are expanded in Fig. 8. Each of these parabolas may be viewed as bands arising from the different degrees of freedom. By examining these band energies E relative to the collective parabolic trend as

$$\Delta E = E - \frac{2\hbar^2}{3I_0}I(I+1) \tag{33}$$

these contributing degrees of freedom can be probed. Note that the second term in eq. 33 comes from the collective rotation of the nucleus based on eq. 9. Plotting this relative energy in Fig. 9, it is seen that for the purple band ΔE roughly equal to zero for all values of I, implying that the dominant contribution is from the collective degree of freedom. However, for the pink band, there is a significant contribution from both single- particle and collective degrees of freedom.

From the diagonalization of eq. 32 the wavefunctions of the lowest-energy state for a given spin are obtained and may be expanded in terms of the basis states as

$$|\Psi IM\rangle = \sum_{J,\Omega} a_{IJ\Omega}|IMj_0j_0J\Omega\rangle \tag{34}$$

where the probability of being in a given basis state is found through the square of the amplitude $a_{IJ\Omega}$ as

$$\text{Probability} = {a_{IJ\Omega}}^2 \tag{35}$$

Of interest are the distributions of probabilities at $I = 14$ and $I = 16$, the region at which the pair break occurs. It is seen in Fig. 10 that for $I = 14$ and below, most of the probability lies in the $J = 0$, $\Omega = 0$ state. However, for $I = 16$ and above, the probability lies over

Fig. 9. The two bands shown in Fig. 8 are now taken relative to the parabolic trend in energy from the collective rotation of the nucleus based on eq. 33. It is seen that the band marked by purple circles is near zero for all values of I, implying that the dominant energetic contribution comes from the collective degree of freedom, whereas the band marked by pink circles has a significant contribution from both collective and single-particle degrees of freedom. The experimental data are also plotted (red crosses) for the lowest-energy state for a given spin, showing agreement with the trends of the predicted bands. [Colour online.]

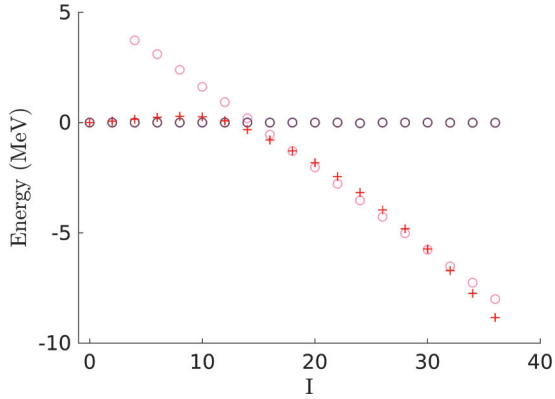

higher angular momentum states. This sudden shift in the probability distribution is further indicative of the pair-breaking effect discussed above. Recall that the Coriolis force decouples the pair from the $J = 0$ state, favouring higher angular momentum states (Fig. 10).

The g factor

The magnetic moment is known to be proportional to the angular momentum of the system,[15] scaled by the gyromagnetic factor (g factor). For the pair of valence nucleons coupled to the axially symmetric rotor, the relevant angular momentum vectors are $\boldsymbol{I}$, $\boldsymbol{J}$, and $\boldsymbol{R}$, which follow the vector addition relation in eq. 24. Subsequently, the observable of the g factor depends on the orientation of the angular momentum vectors in the system. This observable can be measured in nuclei via time-differential perturbed angular distribution.[16] The g factor is related to the diagonal matrix element of the M1 operator.[9] Note, that there are no M1 transitions and off-diagonal matrix elements of M1 since the states differ by 2 in spin and the selection rule requiring $\Delta I = 0, \pm 1$ eliminates the M1 transitions. However, the diagonal M1 matrix element is nonvanishing and is an observable.

First, we begin with the relation

$$\boldsymbol{\mu} = g\frac{\mu_N}{\hbar}\boldsymbol{I} \tag{36}$$

which can be expressed in terms of the expectation values of operators as

$$g = \left\langle \frac{\hbar}{\mu_N}\boldsymbol{\mu}\cdot\boldsymbol{I}\right\rangle \Big| \langle I^2\rangle \tag{37}$$

$$\frac{\hbar}{\mu_N}\boldsymbol{\mu} = g_R\boldsymbol{R} + g_1\boldsymbol{j_1} + g_2\boldsymbol{j_2} \tag{38}$$

where $\boldsymbol{\mu}$ is the vector of the magnetic moment, μ_N is the nuclear magneton, g_R is the gyromagnetic factor for the core rotation, and g_1 and g_2 are gyromagnetic factors for the particles.

The parameters g_R, g_1, and g_2 can be found from experiment. In crude approximation, $g_R = (Z-2)/(A-2)$,[17] where Z is the atomic

Fig. 10. From the model wavefunctions, the probability distributions are shown for $I = 2$ (top left), $I = 14$ (top right), $I = 16$ (bottom left), and $I = 36$ (bottom right). For $I = 14$ and below, most of the probability is with the $J = 0$, $\Omega = 0$ state, whereas for $I = 16$ and above, the probability is distributed more about the higher angular momentum states. This is indicative of the pair breaking occurring between these two spins.

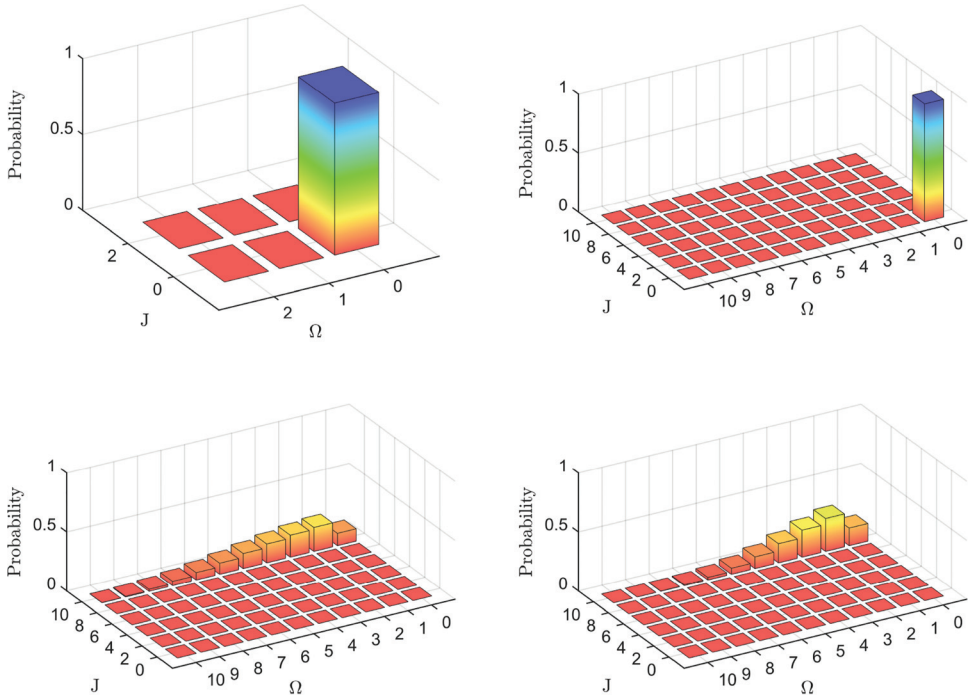

number of the nucleus and A is its mass number. Next, g_1 and g_2 are $g_i = a(g_{\text{free}})$, where g_{free} is the g factor for the valence nucleon, and a is an attenuation factor related to the impact of the medium on the magnetic moment of a free nucleon, which may also be extracted from experiment.

Next, using the substitution $\boldsymbol{R} = \boldsymbol{I} - \boldsymbol{J}$ and noting that for identical valence protons, $g_1 = g_2 = g_p$

$$g_1\boldsymbol{j_1} + g_2\boldsymbol{j_2} = g_p\boldsymbol{J} \tag{39}$$

This simplifies eq. 37, yielding

$$g = \frac{g_R\langle \boldsymbol{I}\cdot\boldsymbol{R}\rangle + g_p\langle \boldsymbol{I}\cdot\boldsymbol{J}\rangle}{\langle I^2\rangle} \tag{40}$$

equivalent to

$$g = \frac{g_R\langle I^2\rangle + (g_p - g_R)\langle \boldsymbol{I}\cdot\boldsymbol{J}\rangle}{\langle I^2\rangle} = g_R + (g_p - g_R)\frac{\langle \boldsymbol{I}\cdot\boldsymbol{J}\rangle}{\langle I^2\rangle} \tag{41}$$

For ^{126}Ce, the g factor is calculated and plotted in Fig. 11, using $Z = 58$, $A = 126$, $a = 0.65$, and $g_{\text{free}} = 5.6$, as well as the wavefunctions from the diagonalization of eq. 32, as a function of I. It is seen that for $I \leq 14$, the predicted g factor is roughly constant with a value of $g = 0.45$. However, for $I \geq 16$, the g factor takes on a different trend, as seen in Fig. 11. This is a result of the pair-breaking effect, in which the angular momentum vectors in the system realign. Effectively, this realignment changes the value of $\boldsymbol{I}\cdot\boldsymbol{J}$, which is used to calculate g, defined in eq. 41. From the probability distributions in Fig. 10, it is seen that for $I \leq 14$, the dominant state is of $J = 0$, $\Omega = 0$, meaning that $\langle \boldsymbol{I}\cdot\boldsymbol{J}\rangle \sim 0$, and $g \sim g_R$ resulting in a constant trend over I. Similarly, as the probability distribution shifts to favour larger values of J, Ω at $I \geq 16$, the $\langle \boldsymbol{I}\cdot\boldsymbol{J}\rangle$ term becomes significantly larger than zero, changing the behaviour of g as a function of I.

Fig. 11. Using the model wavefunctions resultant from the diagonalization of eq. 32, the g factor is calculated from eq. 41 using $Z = 58$, $A = 126$, $a = 0.65$, and $g_{\text{free}} = 5.6$. Note that after the pair break, the g factor changes its trend significantly, due to the realignment in angular moment vectors. [Colour online.]

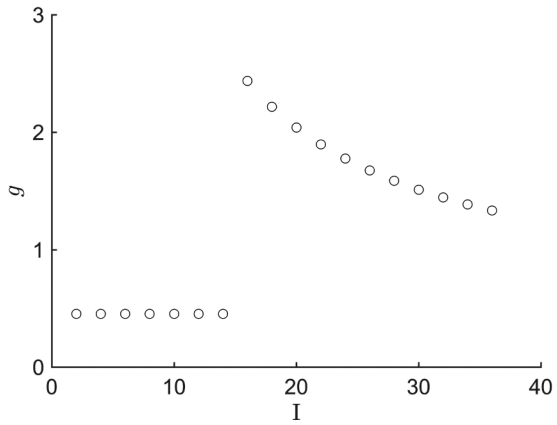

Reduced electric quadrupole transition probability

To calculate the reduced electric quadrupole transition probability from state I_i to I_f, B(E2; $I_i \rightarrow I_f$), the electric quadrupole tensor needs to be calculated. In the intrinsic frame, the electric quadrupole tensor $\mathcal{Q}_{2\nu}$ takes the form

$$\mathcal{Q}_{2\nu} = \sqrt{\frac{16\pi}{5}}\int \rho r^2 Y_{2\nu} dV \tag{42}$$

where the charge density ρ is taken to be a constant over the volume of the axially deformed rotor, the radius of which is parametrized through eq. 2. For the deformed rotor in the pair-rotor

model, when then charge density is integrated over the volume of the body

$$\int \rho dV = (Z - 2)e \tag{43}$$

because there are $Z - 2$ protons in the deformed rotor. However, this tensor in the intrinsic frame needs to be transformed into the lab frame by use of the Wigner D function through the transformation

$$\mathcal{Q}_{2\mu} = \sum_{\nu} D^2_{\mu\nu} \mathcal{Q}_{2\nu} \tag{44}$$

Making use of eqs. 42–44

$$\begin{aligned} \mathcal{Q}_{2\mu} &= e\mathcal{Q}_0 D^2_{\mu 0} \\ \mathcal{Q}_0 &= \frac{3\,(Z - 2)\,R_0^2\beta}{\sqrt{5\pi}} \end{aligned} \tag{45}$$

With the quadrupole moment expressed in this way, the $B(E2)$ values may be derived. The reduced transition probability $B(E2)$ takes the form

$$B(E2; I_i \rightarrow I_f) = \frac{5}{16\pi(2I + 1)} \sum_{\mu,M',M} \left|\langle \Psi I'_f M' | \mathcal{Q}_{2\mu} | \Psi I_i M \rangle\right|^2 \tag{46}$$

which by use of the Wigner–Eckhart theorem becomes

$$B(E2; I_i \rightarrow I_f) = \frac{5}{16\pi(2I + 1)} \left|\langle \Psi I'_f \| \mathcal{Q}_2 \| \Psi I_i \rangle\right|^2 \tag{47}$$

in analogue to the result derived by Davydov and Filippov.[18] Note that in this calculation, the valence pair's contribution to the quadrupole tensor is not included as an approximation, yielding a simplified matrix element. This approximation is justified, because when calculated, the pair's contribution to the quadrupole tensor is negligible compared with the rotor's contribution to the quadrupole tensor.

In Fig. 12, the $B(E2)$ calculation for the pair of interacting valence nucleons coupled to the axial rotor using eq. 34 is compared with the $B(E2)$ using the rotor-only wavefunction of eq. 8. Up to the $I = 14 \rightarrow I = 12$ transition, the $B(E2)$ for the rotor matches the $B(E2)$ for the rotor plus the valence pair, which is expected as the valence pair is coupled to the $J = 0$, $\Omega = 0$ state, based on the probability distributions in Fig. 10. At the transition from $I = 16$ to $I = 14$, the $B(E2)$ for the rotor plus the pair is nearly zero, in contrast to the smooth trend for the rotor-only $B(E2)$. This is because at the pair breaking, the angular momentum jumps from favouring $J = 0$, $\Omega = 0$ to favouring the $J = 8$ and $J = 10$ states, an angular momentum difference greater than 2. However, the $E2$ selection rules allow for a change in angular momentum up to 2, meaning the contribution to the $I = 16 \rightarrow I = 14$ transition from the basis states with the greatest amplitude is zero. After this transition, the trend becomes smooth approaching the rotor-only calculation for increasing I. This behaviour is a result of the rotor's angular momentum $\boldsymbol{R}$ having a larger relative contribution to the total angular momentum $\boldsymbol{I}$ as I increases.

Spectroscopic quadrupole moment

Another observable calculable from the model wavefunctions as a function of I is the spectroscopic electric quadrupole moment. The spectroscopic quadrupole moment $\mathcal{Q}$ is equivalent to the diagonal element of the quadrupole operator discussed above. In the preceding section, it was the off-diagonal matrix elements that were involved in electric quadrupole transitions. This diagonal moment takes the form

$$\mathcal{Q} = \langle \Psi IM = I | \mathcal{Q}_{20} | \Psi IM = I \rangle \tag{48}$$

Once again, the valence pair's negligible contribution to the quadrupole moment is not included in the calculation. Plotting $\mathcal{Q}$ as a function of I in Fig. 13, it is evident there is a distinct change in the trend of this observable as a function of I, despite being a diagonal matrix element of the quadrupole moment operator. However, in contrast to the other observables calculated above, the change in trend is not as pronounced. Again, the changing trend in $\mathcal{Q}$ as a function of spin results from the change in probability distributions about the pair-breaking between $I = 14$ and $I = 16$, as shown in Fig. 10.

Fig. 12. The $B(E2)$ values between states of different I are plotted in units of $e^2\,\mathcal{Q}_0{}^2$. Here, the blue circles are calculated for the axial rotor model using the rotor-only wavefunction of eq. 8, and the red circles are for the pair-rotor coupling model for interacting nucleons using eq. 34. [Colour online.]

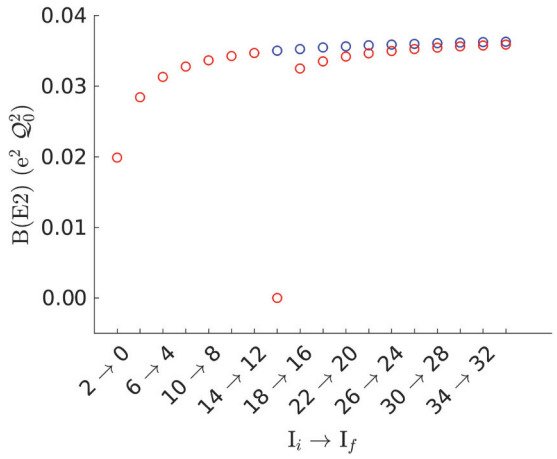

Fig. 13. The quadrupole moment for the axial rotor with interacting valence nucleons is calculated as a function of I using eq. 48 in units of $\mathcal{Q}_0$. Here, the change in the trend of $\mathcal{Q}$ as a function of I after the pair break is less pronounced than for the $B(E2)$.

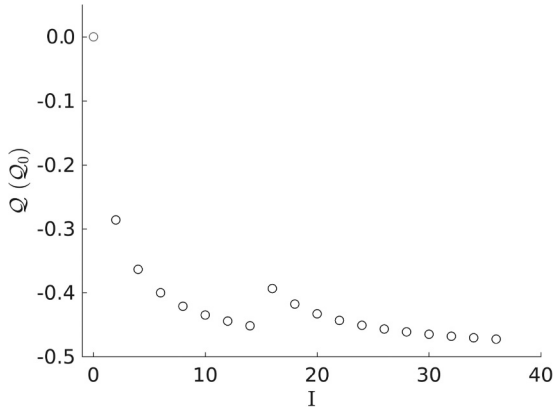

Summary and future work

^{126}Ce was modelled as an axially deformed rotor coupled to a pair of valence nucleons of the same kind to explore the impact of the nuclear Jahn–Teller effect on the single-particle and collective

degrees of freedom in atomic nuclei. As expected, the spontaneous breaking of spherical symmetry in atomic nuclei has an impact on single-particle degrees of freedom through interactions of valence nucleons with the deformed mean field and through the contact nucleon–nucleon interactions, whereas the collective degrees of freedom are impacted through the magnitude of the moment of inertia. The coupling between the single-particle and collective degrees of freedom is best manifested through the Coriolis interactions of the angular momenta of the valence pair and the rotor. Encapsulated in this toy model are the two opposing driving forces for the single particles: the pair-breaking Coriolis force and the pairing nuclear delta force. Modelling both of these opposing forces allows agreement with the data.

The two opposing forces acting on the valence pair of nucleons, the Coriolis force and the nuclear delta force, are of comparable magnitude, and both make a significant impact on the state of the system near the pair breaking. This phenomenon is unique when compared with other quantum systems, like molecules, because it is only in nuclei where occupation of high-spin nucleon states like $h_{11/2}$ is allowed. A pair of $h_{11/2}$ nucleons can couple to J between 0 and 10. For a given angular momentum, this pair interacts at an energy scale comparable with that of the collective rotation of the nucleus. This is very different than in molecules, where the collective rotation of the molecule as a whole dominates the angular momentum and the energy scale associated with the rearrangement of electrons in valence shells is a minute effect in comparison.

Using the model wavefunction observables including the g factor, the reduced electric quadrupole transition probability, and the spectroscopic quadrupole moment were calculated as a function of spin. In each case, the pair-breaking played a role resulting in a distinct change in the trend of predicted values as functions of spin. Due to the lack of data for these observables, chiefly at the region of the pair breaking, these calculations serve as a prediction to be tested experimentally.

In future studies, a similar analysis will be carried out for the triaxial quadrupole deformed rotor to reproduce the data and probe and understand the relevant physical systems. The rotor-pair coupling model may also be extended to encompass higher order deviations from the spherical shape and tested by the same procedure as outlined here for the axially symmetric quadrupole deformation.

References

(1) Reinhard, P.-G.; Otten, E. W. *Nucl. Phys. A* **1984**, *420*, 173. doi:10.1016/0375-9474(84)90437-8.
(2) Satuła, W.; Dobaczewski, J.; Nazarewicz, W. *Phys. Rev. Lett.* **1998**, *81*, 3599. doi:10.1103/PhysRevLett.81.3599.
(3) Inglis, D. R. *Phys. Rev.* **1956**, *103*, 1786. doi:10.1103/PhysRev.103.1786.
(4) Long, W. H.; Ring, P.; Van Giai, N.; Meng, J. *Phys. Rev. C* **2010**, *81*, 024308. doi:10.1103/PhysRevC.81.024308.
(5) Hamamoto, I. *Nucl. Phys. A* **1976**, *271*, 15. doi:10.1016/0375-9474(76)90264-5.
(6) Frauendorf, S.; Meng, J. *Nucl. Phys. A* **1997**, *617*, 131. doi:10.1016/S0375-9474(97)00004-3.
(7) Yadav, H. L.; Toki, H.; Faessler, A. *Phys. Rev. Lett.* **1977**, *39*, 1128. doi:10.1103/PhysRevLett.39.1128.
(8) Bohr, A.; Mottelson, B. R. *Nuclear Structure: Volume 2, Nuclear Deformations*; W.A. Benjamin: New York, 1975.
(9) Bohr, A.; Mottelson, B. R. *Nuclear Structure: Volume 1, Single-Particle Motion*; W.A. Benjamin: New York, 1969.
(10) Katakura, J.; Kitao, K. *Nucl. Data Sheets* **2002**, *97*, 765. doi:10.1006/ndsh.2002.0020.
(11) Varshalovich, D. A.; Moskalev, A. N.; Khersonskii, V. K. *Quantum Theory of Angular Momentum*; World Scientific: Singapore, 1988.
(12) Kay, K. G.; Todd, H. D.; Silverstone, H. J. *J. Chem. Phys.* **1969**, *51*, 2359. doi:10.1063/1.1672352.
(13) Sonzogni, A. A. *Nucl. Data Sheets* **2004**, *103*, 1. doi:10.1016/j.nds.2004.11.001.
(14) Rekstad, J.; Engeland, T. *Phys. Lett. B* **1980**, *89*, 316. doi:10.1016/0370-2693(80)90132-X.
(15) Hamilton, W. D. *The Electromagnetic Interaction in Nuclear Spectroscopy*; North Holland Publishing Company: Amsterdam, 1975.
(16) Nakai, K.; Skaali, B.; Sigurd Hansen, N. J.; Herskind, B.; Sawa, Z. *Phys. Rev. Lett.* **1971**, *27*, 155. doi:10.1103/PhysRevLett.27.155.
(17) Caurier, E.; Egido, J. L.; Martínez-Pinedo, G.; Poves, A.; Retamosa, J.; Robledo, L. M.; Zuker, A. P. *Phys. Rev. Lett.* **1995**, *75*, 2466. doi:10.1103/PhysRevLett.75.2466.
(18) Davydov, A. S.; Filippov, G. F. *Nucl. Phys.* **1958**, *8*, 237. doi:10.1016/0029-5582(58)90153-6.